Local ionic and electron heating in single-molecule junctions

ZHIFENG HUANG[1], FANG CHEN[1], ROBERTO D'AGOSTA[2], PETER A. BENNETT[3], MASSIMILIANO DI VENTRA[2]* AND NONGJIAN TAO[1]*

[1]Department of Electrical Engineering & The Center for Solid State Electronics Research, Arizona State University, Tempe, Arizona 85287, USA
[2]Department of Physics, University of California, San Diego, La Jolla, California 92093, USA
[3]Department of Physics, Arizona State University, Tempe, Arizona 85287, USA
*e-mail: nongjian.tao@asu.edu; diventra@physics.ucsd.edu

Published online: 28 October 2007; doi:10.1038/nnano.2007.345

A basic aim in molecular electronics is to understand transport through a single molecule connected to two electrodes. Substantial progress towards this goal has been made over the past decade as a result of advances in both experimental techniques and theoretical methods[1–3]. Nonetheless, a fundamental and technologically important issue, current-induced local heating of molecules[4–8], has received much less attention. Here, we report on a combined experimental and theoretical study of local heating in single molecules (6-, 8- and 10-alkanedithiol) covalently attached to two gold electrodes as a function of applied bias and molecular length. We find that the effective local temperature of the molecular junction first increases with applied bias, and then decreases after reaching a maximum. At fixed bias, the effective temperature decreases with increasing molecular length. These experimental findings are in agreement with hydrodynamic predictions, which include both electron–phonon and electron–electron interactions[7,9].

As silicon-based microelectronics continues to miniaturize towards ever smaller scales, heat dissipation is becoming an increasingly important and difficult problem[10]. It has been argued that the mean free path of inelastic scattering of electrons in nanoscale structures, such as a molecular junction, is longer than the dimensions of the devices, so scattering events at the junction are expected to be rare. On the other hand, the small size implies small heat capacity and large current densities, that is, a large number of electron–phonon and electron–electron scattering events per unit time and unit volume in the junction compared to the bulk. Therefore, even a small amount of energy transfer from current-carrying electrons to phonons or other electrons in the molecule or at the molecule–electrode contacts may lead to substantial heating of the device. Furthermore, in a nanoscale structure, the electron screening length is expected to be larger and the current density higher than in bulk metals, which may lead to new phenomena due to stronger electron–electron interactions. Several theoretical papers have been devoted to local heating of a single-molecule junction due to the scattering of electrons by phonons or vibrational modes[5,6], as shown in inelastic tunnelling spectra (IETS)[11–15]. Recently, it has been predicted that transport in nanoscale junctions is accompanied by local heating, with contributions from both electron–phonon and electron–electron scattering processes[9]. The most striking prediction is that, with increasing bias, the electron–electron interactions will eventually 'cool' the ions of the junction; that is, if one were able to measure the local temperature of the ions, it would first increase with the applied bias, and then decrease after reaching a maximum value. In this paper we report on experimental evidence of such effect.

Direct measurement of local heating of a single-molecule junction has been difficult due to the lack of experimental techniques. Evidence of local ionic heating has been provided by measuring the bond rupture force of individual molecular junctions using conducting atomic force microscopy (C-AFM)[8]. In the present work, we study local heating by measuring the mechanical stretching distance of single molecular junctions using a scanning tunnelling microscopy (STM) break junction. This technique allows us to determine the effective local temperature as a function of applied bias and molecular length, and observe evidence of both ionic and electron heating.

To investigate the local-heating effect, we chose *n*-alkanedithiol (HS–$(CH_2)_n$–SH or C*n*, where $n = 6$, 8 and 10) for the following reasons. First, electron transport through these molecules is well described by elastic tunnelling or super-exchange processes, and the molecular length dependence of the conductance (G) is given by $G = Ae^{-\beta n}$, where A is a constant and β a decay coefficient possibly depending on the applied bias. Second, the length of *n*-alkanedithiols can be systematically varied by changing the number of C atoms in the chain without changing the electron transport mechanism. Third, current-induced forces are expected to be negligible for these molecules in the range of biases considered here because of the small tunnelling current through the molecular junctions[8,16]. Finally, the molecules are terminated with dithiols, which can bind to gold electrodes through the Au–S bond and form Au–molecule–Au junctions. By pulling the two electrodes apart, each molecular junction is stretched and eventually breaks (Fig. 1a). We have shown previously that the stretching takes place primarily at the electrode–molecule contacts, and the final breakdown is due to the rupture of the Au–Au bond[17]. An important quantity that can be determined by analysing the breakdown of thousands of molecular junctions is the distance L over which the molecular junctions can be stretched before breakdown. As we will show later, the breakdown process is thermally activated; that is, L is directly related to the effective local temperature of the molecule–electrode contacts.

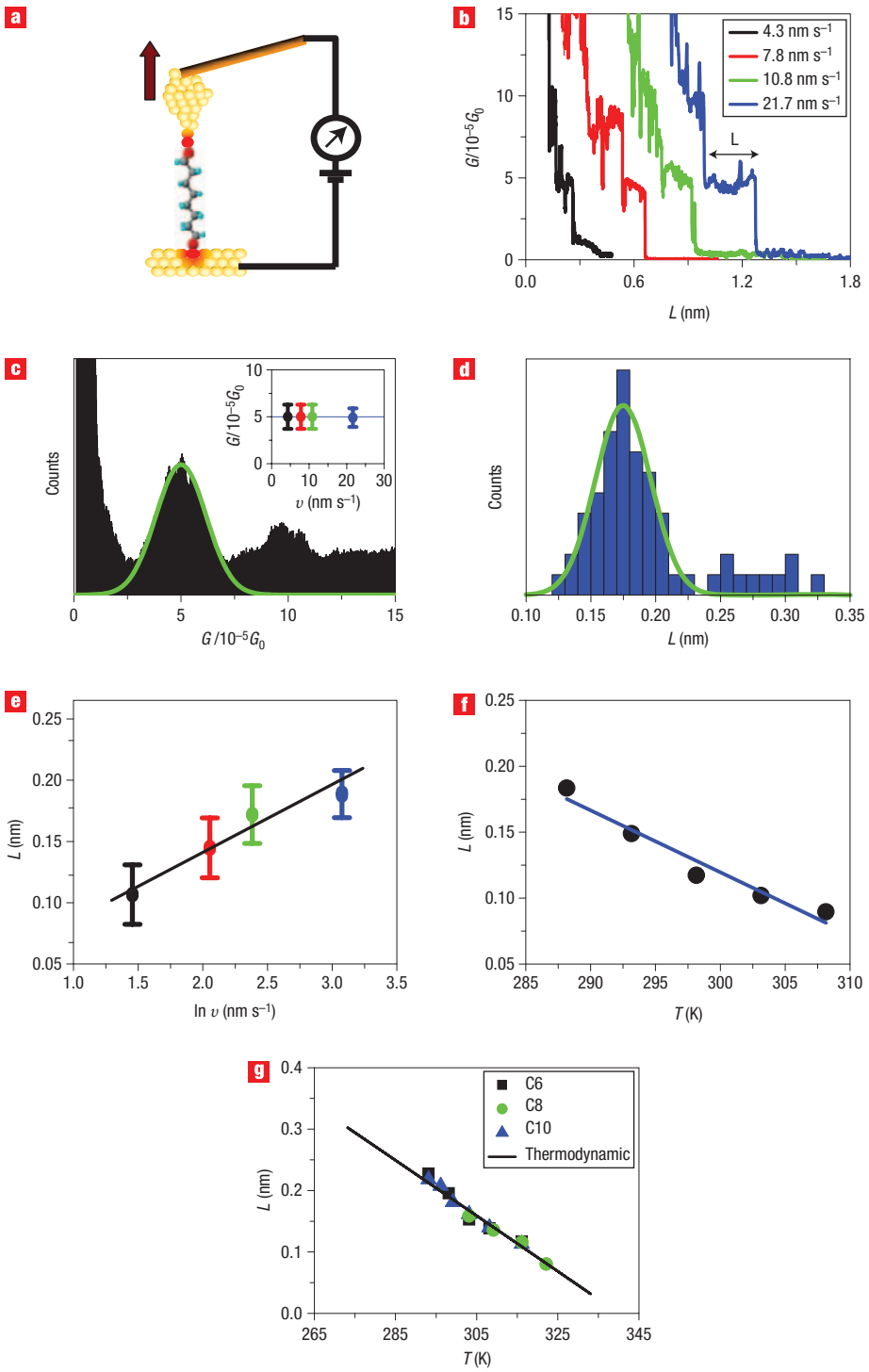

Figure 1 Measurements of conductance and stretching distance of single *n*-alkanedithiol junctions. a, Formation of a single molecule (*n*-alkanedithiol) covalently bound to two gold electrodes through Au–S bonds, using an STM break-junction approach. Continuously pulling the STM tip away from the substrate breaks the molecule junction. **b**, Individual conductance traces during stretching of C8 junctions at room temperature with different stretching rates. The arrow marks the stretching distance of the lowest conductance step, corresponding to a single C8 junction. **c**, Conductance (G) histogram at room temperature (stretching rate = 4.3 nm s^{-1}). The green line is a gaussian fit, and the inset plots the average C8 conductance versus stretching rate. **d**, Stretching distance (L) histogram of C8 at room temperature (stretching rate = 21.7 nm s^{-1}). The green line is a gaussian fit. **e**, Average stretching distance versus log of stretching rate for C8, where the black line is a fit to equation (1). Note that the peak position of the gaussian fit (in **d**) determines the average stretching length, which has an error of ~0.001–0.002 nm, the size of the data points, and the peak width represents the distribution, which is plotted as error bars. **f**, Average stretching distance versus temperature for C8 (stretching rate = 7.4 nm s^{-1}). The blue line is a fit to equation (1). **g**, Average stretching distance versus controlled temperature for C6, C8 and C10 (stretching rate = 20 nm s^{-1}). The solid line is calculated using equation (1), which is in good agreement with the experimental data. The applied bias voltages in all the measurement were kept small (100 mV for C8 and C10 and 50 mV for C6).

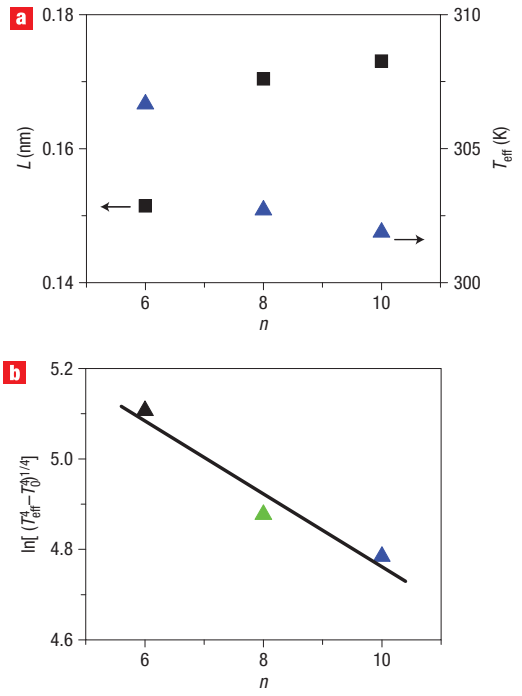

Figure 2 Measurements of stretching distance and effective temperature of single *n*-alkanedithiol junctions (n = 6, 8, 10) at small voltage bias. **a**, Plot of average stretching distance (L) versus molecular length (n) (black squares) and effective temperature (T_{eff}) versus n (blue triangles). **b**, Semi-logarithmic plot of $(T_{eff}^4-T_0^4)^{1/4}$ with n, linearly fitted with the black line. T_0 is the ambient temperature, 300 K. All the measurements are carried out at room temperature with the stretching rate fixed at 20 nm s^{-1} and the applied bias at 100 mV.

Figure 1b shows the conductance traces transiently monitored during stretching of individual molecular junctions at different stretching rates, where the last steps correspond to the formation and breakdown of the single molecular junctions. A histogram of the step positions has been constructed from ~30–40% of ~2,000 transient curves showing steps at a given stretching rate and bias (Fig. 1c). The peak at the lowest conductance provides the average conductance of a single molecule, which is $\sim 5 \times 10^{-5} G_0$ ($G_0 = 2e^2/h$, where e is the electron charge and h is the Planck constant) for C8. The average conductance is independent of stretching rate (inset of Fig. 1c). We have also analysed the distribution of the stretching distance L, which also shows a peak in the histogram (Fig. 1d). Unlike the conductance, the peak position of the stretching distance distribution, corresponding to the average stretching distance, is sensitive to the stretching rate (Fig. 1e). The dependence of the stretching distance on stretching rate is due to thermally activated bond-breaking processes. According to a thermodynamic theory developed by Evans[18], the average stretching distance can be written as (see Methods)

$$L = \frac{E_b}{x_\beta k_s} + \frac{k_B T_{eff}}{x_\beta k_s} \ln\left(\frac{x_\beta k_s t_D}{k_B T_{eff}} v\right) \quad (1)$$

where E_b is the dissociation energy barrier, x_β is the average thermal bond length along the stretching direction until rupture, T_{eff} is the effective temperature, t_D is the diffusion relaxation time, k_B is the Boltzmann constant, and k_s is the effective spring constant. The logarithmic dependence of stretching distance on the stretching rate predicted by the theory is in good agreement with our data (Fig. 1e). To further confirm that the bond breakdown is thermally activated, we have measured the stretching distance as a function of temperature at a given small bias and found that this length decreases with temperature (Fig. 1f).

The measured stretching distance versus stretching rate shown in Fig. 1e can be fitted using equation (1), and $x_\beta k_s$ is found to be 73.5 pN. Note that the data in Fig. 1e have been obtained at a small bias (100 mV), so no substantial local heating is present[8]. By fitting the temperature dependence of the stretching distance shown in Fig. 1f with equation (1), E_b and t_D are found to be 0.68 eV and 0.28 ps, respectively. Both the binding energy E_b and relaxation time t_D are in good agreement with the previous C-AFM measurement[8], and support the conclusion that the rupture of single n-alkanedithiol junctions most likely takes place at the Au–Au bond. We have also measured the stretching distance versus temperature and versus stretching rate for C6 and C10. The measured stretching distances are similar for all the molecules, and the parameters E_b, $x_\beta k_s$ and t_D are independent of molecular length (Fig. 1g; see also Supplementary Information, Fig. S1). This again is consistent with the observation that the rupture of these molecular junctions takes place at the Au–Au bonds near the molecule–electrode contacts.

The measured average stretching distance versus temperature, shown in Fig. 1g, can be used to extract T_{eff} from the average stretching distance. A different approach to determine T_{eff} is to use the thermodynamic theory of equation (1). Using the parameters determined above, a calibration curve in temperature versus average stretching length has been obtained (solid black curve in Fig. 1g). The calibration curve is consistent with the directly measured results for all three molecules, which allowed us to determine T_{eff} as a function of bias voltage V_{bias} for the molecules of different lengths.

It was predicted that the effective local temperature T_{eff} of the ions changes with bias, for $V_{bias} < (\gamma_{e\text{-}p}/\gamma_{e\text{-}e})^2$, as[7]

$$T_{eff}^4 = T_0^4 + \gamma_{e\text{-}p}^4 V_{bias}^2 - \gamma_{e\text{-}e}^4 V_{bias}^4 \quad (2)$$

where $\gamma_{e\text{-}p}$ and $\gamma_{e\text{-}e}$ describe the heat contribution due to the electron–phonon and electron–electron interactions, respectively. Both these parameters may vary with bias if the conductance varies with bias. T_0 is the ambient temperature. Equation (2) shows that at low biases, the electron–phonon contribution to the ionic temperature dominates. As the bias increases, the electron–electron interaction effects increase in importance, by effectively cooling the ionic lattice. The reason for this behaviour is related to the fact that when electrons traverse from one electrode to the other across the molecule, a portion of their energy is transferred to the ionic degrees of freedom through electron–phonon interactions, and another portion to the electronic degrees of freedom through electron–electron interactions; that is, the underlying Fermi gas heats up. With increasing bias, the current-carrying electrons transfer an ever increasing energy (which is then not available to heat the ions) to the other electrons in the molecule and in the electrodes connected to the molecule. As the heated electrons carry energy away from the molecular junction and eventually dissipate it to the bulk of the electrodes, the electron heating effect lowers the effective temperature of the ionic degrees of freedom in the molecular junction. We note that due to a much greater ionic

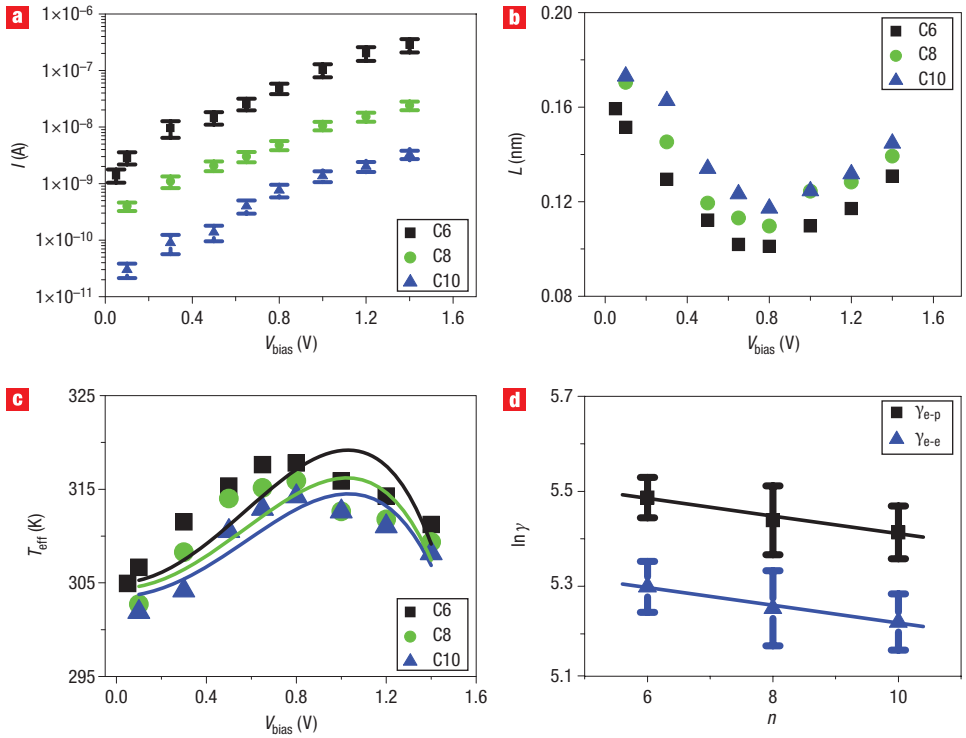

Figure 3 Measurements of stretching distance and effective temperature of single *n*-alkanedithiol (*n* = 6, 8, 10) junctions with increasing voltage bias. **a**, Current through the single-molecule junctions versus applied bias V_{bias}. **b**, Average stretching distance (L) versus bias. **c**, Effective temperature (T_{eff}) versus bias; the black (C6), green (C8) and blue (C10) curves are the fits from equation (2). **d**, Semi-logarithmic plots of $\gamma_{e\text{-}p}$ (black squares) and $\gamma_{e\text{-}e}$ (blue triangles) versus molecular length, linearly fitted with the black and blue lines, respectively. All the measurements were carried out at room temperature with the stretching rate fixed at 20 nm s^{-1}.

heating effect in metallic point contacts, the cooling effect becomes pronounced only at very high biases, where current induced forces would cause breakdown of the contacts. This is likely the reason for the lack of cooling effect in the study of local heating effects in metallic point contacts[19].

Let us first focus on the molecular length dependence of the local-heating effect at a small fixed bias of 100 mV. Figure 2a shows the stretching distance of C6, C8 and C10 at this bias. Using the calibration curve in Fig. 1g, T_{eff} values have been extracted from the stretching distance as a function of n, the number of C atoms in the alkanedithiol (Fig. 2a). The result shows that shorter molecules have higher local temperature, in agreement with the theoretical prediction[6]. At low bias, electron–phonon interactions are the primary source of local heating in equation (2), and T_{eff} may be reasonably described as

$$T_{eff}^4 = T_0^4 + \gamma_{e\text{-}p}^4 V_b^2 \qquad (3)$$

According to ref. 6, the molecular length dependence of $\gamma_{e\text{-}p}$ in the absence of electron heating and at small biases is

$$\gamma_{e\text{-}p}(n) = \gamma_{e\text{-}p}(0)e^{-\beta_1 n} \qquad (4)$$

where $\gamma_{e\text{-}p}(0) = 375$ K $V^{-1/2}$ is a constant, with $\beta_1 = 0.19$ per C atom a decay coefficient. Figure 2b reports a semi-logarithmic plot of $(T_{eff}^4 - T_0^4)^{1/4}$ versus n, showing an exponential dependence of $(T_{eff}^4 - T_0^4)^{1/4}$ on molecular length, n. By fitting the data with equation (4), we found that $\beta_1 = 0.08$ per C atom and $\gamma_{e\text{-}p}(0)$ was 828 K $V^{-1/2}$ at 100 mV. As we will discuss later, much smaller values of $\gamma_{e\text{-}p}(0)$ and β_1 are obtained when we consider the complete expression in equation (2) for the local ionic heating. This indicates that the effect of local electron heating cannot be neglected even at small biases.

To investigate the bias-dependent local-heating effect, we have obtained the I–V characteristics of molecules with different lengths by creating conductance histograms at various biases for each of the molecules (see Supplementary Information, Fig. S2). The current increases linearly with the bias below 0.5 V, then more rapidly above 0.5 V (Fig. 3a), which is expected from the Simmons tunnelling model[20]. We have also measured the stretching distance as a function of bias for the molecules (Fig. 3b). For biases less than 0.8 V, the stretching distance decreases with bias and the corresponding T_{eff} increases with bias as shown in Fig. 3c. This behaviour is expected, as a higher bias leads to higher current and thus more local heating. By increasing the bias above ~0.8 V, T_{eff} reaches a plateau, and then begins to decrease as predicted by equation (2). Note that other possible effects contributing to the rupture of the junction, such as current-induced forces, would effectively increase the local ionic temperature. Compared to the C-AFM measurement[8], T_{eff} for C8 in the present work is slightly lower, due to the presence of greater experimental errors in the C-AFM results.

The electron–electron interaction constant $\gamma_{e\text{-}e}$ in equation (2) is given by (see Methods)

$$\gamma_{e\text{-}e}(n) = \gamma_{e\text{-}e}(0)e^{-\beta_2 n} \qquad (5)$$

where $\gamma_{e\text{-}e}(0)$ is a constant and β_2 is a decay coefficient. Equation (2), together with equations (4) and (5), explains the observed dependence of T_{eff} on bias and molecular length. A quantitative comparison between the theory and experiment is difficult due to the unknown bias dependence of β_1, β_2 and the electron viscosity, which enters the parameter $\gamma_{e\text{-}e}$. However, even if we assume that all these parameters are independent of bias, equation (2) provides a reasonable fit of the data, shown in Fig. 3c. Values of $\gamma_{e\text{-}p}$ for C6, C8 and C10 are found to be 239 ± 10, 228 ± 17 and 222 ± 12 K $V^{-1/2}$, respectively, and for $\gamma_{e\text{-}e}$ are 198 ± 11, 189 ± 15 and 184 ± 11 K V^{-1}, respectively. Figure 3d shows the linear fit with the semi-logarithmic of $\gamma_{e\text{-}p}$ and $\gamma_{e\text{-}e}$ with n, to extract $\gamma_{e\text{-}p}(0) = 267 \pm 36$ K $V^{-1/2}$, $\beta_1 = 0.019$, $\gamma_{e\text{-}e}(0) = 221 \pm 35$ K V^{-1} and $\beta_2 = 0.006$. The theory predicts $\gamma_{e\text{-}e}(0) = 92$ K V^{-1} for this system[7]. We stress here that our experiment effectively measures the temperature of the contact between molecule and electrodes at the breaking point, but the theoretical values refer to the average temperature in the molecule covalently attached to the electrodes. Therefore, the agreement between experiment and theory is reasonably good, with the experimental value for $\gamma_{e\text{-}e}(0)$ about a factor of two larger than the theoretical estimate. Furthermore, we note that the experimental results do clearly show the cooling effect predicted theoretically.

In summary, we have determined the effective temperature of single-molecule (n-alkanedithiol) junctions due to current-induced local heating as a function of molecular length and applied bias voltage. Our method is based on analysing the average stretching length over which a molecular junction can be stretched before breakdown, using the STM break junction approach. By measuring the stretching length as a function of stretching rate and temperature, we have shown that the breakdown of the molecular junctions is thermally activated and the dependence of the stretching length on temperature is used to extract the effective temperature of single-molecule junctions. We have reported the following noteworthy findings that confirm the predictions of a hydrodynamic approach to transport that takes into account both electron–phonon and electron–electron interactions: (1) At a given bias, the local ionic heating increases with decreasing molecular length; (2) For a given molecule, the effective local ionic temperature first increases with bias, and then decreases after reaching a maximum value at ~0.8 V. This effective cooling of the ionic temperature at high biases is due to electron–electron interactions with consequent local electron heating at the junction.

METHODS

EXPERIMENTAL DETAILS

STM tips were prepared by freshly cutting Au wires (99.998%) with a diameter of 0.25 mm. The sample cell was made of Teflon cleaned in boiling Piranha (98% H_2SO_4:30%H_2O_2 = 3:1, v/v) for ~30 min, and then thoroughly rinsed in boiling water (18 MΩ, Nanopure system fed with campus distilled water) three times. (Caution: Piranha reacts violently with most organic materials, so extreme care should be taken when handling it.) Au substrates were prepared by thermally evaporating 130 nm gold (99.999%) on freshly cleaved micas in an ultra high vacuum chamber. Before each experiment, a substrate was annealed with a H_2 flame for ~1 min, and then immediately immersed in toluene with 1 mM n-alkanedithiol (n = 6, 8, 10) in the sample cell. The temperature of the Au substrates was controlled by a Peltier stage (Molecular Imaging, approx. −5 to 40 °C) and a high-temperature stage (Molecular Imaging, ambient ~170 °C). All the measurements were performed in toluene.

REPEATED FORMATION AND RUPTURE OF SINGLE-MOLECULE JUNCTIONS

An STM break junction approach was used to repeatedly create and break single-molecule junctions[21,22]. The process started with a H_2-annealed Au substrate covered with a layer of n-alkanedithiol adsorbed onto the substrate from toluene. An Au STM tip was then brought into gentle contact with the substrate, during which time multiple molecules were able to bridge between the tip and substrate electrodes through Au–S bonds. The tip was then pulled away from the substrate, sequentially breaking individual molecular junctions formed during the contact. After breaking the last molecular junction, the above process was repeated to form and break a large number of molecule junctions. The repeated dissociation processes were transiently monitored through the stepwise decrease of conductance. Statistical analysis of the position and length of the lowest conductance steps provided the most probable conductance and stretching distances of the single-molecule junctions.

The distribution of the stretching distance can be fitted with a gaussian function (Fig. 1d; see also Supplementary Information, Fig. S3). The position gives the most probable stretching distance, with a small error (for example, ~0.001–0.002 nm in Fig. 1e), resulting in a negligible error in temperature T_{eff}. The width reflects the variation in the distance due to different molecule–electrode contact configurations. An alternative way to analyse the stretching distance is to add up all the step lengths of all the curves that exhibit well-defined conductance steps and then divide this total by the number of curves to obtain the average stretching distance. Both approaches yield similar results, due to the approximately symmetric distribution in the histograms (see Supplementary Information, Fig. S3).

THERMODYNAMIC THEORY OF BOND BREAKDOWN

The breakdown process of a diatomic chemical bond is thermally activated and well described by thermodynamic theory[18,23,24]. According to the theory, the stretching force required to break a chemical bond depends on temperature and on how fast the stretching force is applied. In the so-called linear regime, the most probable breakdown force, F^*, is given by[18,23]

$$F^* = \frac{E_b}{x_\beta} + \frac{k_B T_{eff}}{x_\beta} \ln\left(\frac{x_\beta t_D}{k_B T_{eff}} r_F\right) \quad (6)$$

where r_F is the force loading rate in unit of nN s^{-1}. As the average stretching distance is small (<0.2 nm) compared with that of the Au atomic contact at low temperatures[25], the force is approximately linearly proportional to the stretching length before breakdown of the chemical bond[17], and the most probable stretching length L^* is given by $L^* = F^*/k_s$, where k_s is the effective spring constant of the chemical bond. Equation (6) becomes

$$L^* = \frac{E_b}{x_\beta k_s} + \frac{k_B T_{eff}}{x_\beta k_s} \ln\left(\frac{x_\beta k_s t_D}{k_B T_{eff}} v\right) \quad (7)$$

where v is the stretching rate in unit of nm s^{-1}, with $v = r_F/k_s$. Owing to the approximately symmetric distribution of the stretching distance (see Supplementary Information, Fig. S3), L^* is roughly equal to the average L, so we obtain equation (1).

MICROSCOPIC THEORY FOR $\gamma_{e\text{-}e}$

If we assume that the molecular junction is adiabatically connected to the leads through the Au–S bonds, we predict, using a hydrodynamic theory of the electron liquid[9], that $\gamma_{e\text{-}e}$ depends linearly on the conductance G of the device, namely[7,9]

$$\gamma_{e\text{-}e} \propto \frac{G}{\rho e A} \sqrt{\frac{\eta}{\gamma}} \quad (8)$$

where A is the molecular cross-section, η is the electron viscosity, ρ is the electron density in the junction, and γ is a constant related to the specific heat of the system[7]. Both η and γ may have a non-trivial dependence on bias and molecular length. When studying the effect of the local electron heating alone, a simple argument gives us the relation (assuming zero background temperature)[7]

$$T_{eff} = \gamma_{e\text{-}e} V_{bias} \quad (9)$$

The electron viscosity is a functional of the density ρ, and its numerical values are available in tabulated form (see ref. 7 and references therein). The electron gas in the molecule acts as an energy sink from the point of view of the phonon modes of the molecular junction. This explains the origin of the minus sign in equation (2). As both G and γ depend on the length of the molecule, from equation (9), we expect that $\gamma_{e\text{-}e}$ scales exponentially (see equation (5)) with the

length of the molecular junction. β_2 is a decay coefficient not necessarily equal to the decay constant β_1 appearing in the electron–phonon coupling. The determination of β_2 is non-trivial, as one needs to know the length dependence of the electron viscosity, density and specific heat at any bias. From equation (2) and using equations (4) and (5), we also predict that the bias at which the maximum temperature is reached increases with the molecular length.

Received 31 July 2007; accepted 26 September 2007; published 28 October 2007.

References

1. Lindsay, S. M. & Ratner, M. A. Molecular transport junctions: Clearing mists. *Adv. Mater.* **19,** 23–31 (2007).
2. Tao, N. J. Electron transport in molecular junctions. *Nature Nanotechnol.* **1,** 173–181 (2006).
3. Selzer, Y. & Allara, D. L. Single-molecule electrical junctions. *Annu. Rev. Phys. Chem.* **57,** 593–623 (2006).
4. Todorov, T. N. Local heating in ballistic atomic-scale contacts. *Phil. Mag. B* **77,** 965–973 (1998).
5. Segal, D. & Nitzan, A. Heating in current carrying molecular junctions. *J. Chem. Phys.* **117,** 3915–3927 (2002).
6. Chen, Y. C., Zwolak, M. & Di Ventra, M. Local heating in nanoscale conductors. *Nano Lett.* **3,** 1691–1694 (2003).
7. D'Agosta, R., Sai, N. & Di Ventra, M. Local electron heating in nanoscale conductors. *Nano Lett.* **6,** 2935–2938 (2006).
8. Huang, Z. F., Xu, B. Q., Chen, Y. C., Di Ventra, M. & Tao, N. J. Measurement of current-induced local heating in a single molecule junction. *Nano Lett.* **6,** 1240–1244 (2006).
9. D'Agosta, R. & Di Ventra, M. Hydrodynamic approach to transport and turbulence in nanoscale conductors. *J. Phys. Condens. Matter.* **18,** 11059–11065 (2006).
10. Bechtold, T., Rudnyi, E. B. & Korvink, J. G. Dynamic electro-thermal simulation of microsystems—a review. *J. Micromech. Microeng.* **15,** R17–R31 (2005).
11. Solomon, G. C. *et al.* Understanding the inelastic electron-tunneling spectra of alkanedithiols on gold. *J. Chem. Phys.* **124,** 094704 (2006).
12. Wang, W. Y., Lee, T., Kretzschmar, I. & Reed, M. A. Inelastic electron tunneling spectroscopy of an alkanedithiol self-assembled monolayer. *Nano Lett.* **4,** 643–646 (2004).
13. Kushmerick, J. G. *et al.* Vibronic contributions to charge transport across molecular junctions. *Nano Lett.* **4,** 639–642 (2004).
14. Kaun, C. C. & Seideman, T. Current-driven oscillations and time-dependent transport in nanojunctions. *Phys. Rev. Lett.* **94,** 226801 (2005).
15. Kaun, C. C., Jorn, R. & Seideman, T. Spontaneous oscillation of current in fullerene molecular junctions. *Phys. Rev. B* **74,** 045415 (2006).
16. Di Ventra, M., Pantelides, S.T. & Lang, N. D. Current-induced forces in molecular wires. *Phys. Rev. Lett.* **88,** 046801 (2002).
17. Xu, B. Q., Xiao, X. Y. & Tao, N. J. Measurements of single-molecule electromechanical properties. *J. Am. Chem. Soc.* **125,** 16164–16165 (2003).
18. Evans, E. Probing the relation between force, lifetime and chemistry in single molecular bonds. *Annu. Rev. Biophys. Biomol. Struct.* **30,** 105–128 (2001).
19. Tsutsui, M., Kurokawa, S. & Sakai, A. Bias-induced local heating in atom-sized metal contacts at 77 K. *Appl. Phys. Lett.* **90,** 133121 (2007).
20. Li, X. *et al.* Conductance of single alkanedithiols: Conduction mechanism and effect of molecule–electrode contacts. *J. Am. Chem. Soc.* **128,** 2135–2141 (2006).
21. Xu, B. Q. & Tao, N. J. J. Measurement of single-molecule resistance by repeated formation of molecular junctions. *Science* **301,** 1221–1223 (2003).
22. Xiao, X. Y., Nagahara, L. A., Rawlett, A. M. & Tao, N. J. Electrochemical gate-controlled conductance of single oligo(phenylene ethynylene)s. *J. Am. Chem. Soc.* **127,** 9235–9240 (2005).
23. Evans, E. & Ritchie, K. Dynamic strength of molecular adhesion bonds. *Biophys. J.* **72,** 1541–1555 (1997).
24. Evans, E. Energy landscapes of biomolecular adhesion and receptor anchoring at interfaces explored with dynamic force spectroscopy. *Faraday Discussions* **111,** 1–16 (1998).
25. Rubio-Bollinger, G., Bahn, S. R., Agrait, N., Jacobsen, K. W. & Vieira, S. Mechanical properties and formation mechanisms of a wire of single gold atoms. *Phys. Rev. Lett.* **87,** 026101 (2001).

Acknowledgements

We thank the US National Science Foundation (ECS0304682, Z.F.H.), the US Department of Energy (DE-FG03-01ER45943, F.C. and Z.F.H.) and (DE-FG02-05ER46204, R.D.) for financial support. Correspondence and requests for materials should be addressed to N.J.T. and M.D.V. Supplementary information accompanies this paper on www.nature.com/naturenanotechnology.

Author contributions

Z.F.H. carried out the experiment and data analysis, F.C. assisted in the experiment, R.D. and M.D.V. worked out the theory and predicted local cooling, P.B. provided important comments and N.J.T. conceived the experiment.